A Computational Model that Predicts how Extracellular Matrix Density Regulates Microvascular Topology during Sprouting Angiogenesis

Lowell T. Edgar[1, 3], Clayton J. Underwood[1, 3], James E. Guilkey[2, 3], Jeffrey A. Weiss[1, 3]

1. Department of Bioengineering, University of Utah, Salt Lake City, UT
2. Department of Mechanical Engineering, University of Utah, Salt Lake City, UT
3. Scientific Computing and Imaging Institute, University of Utah, Salt Lake City, UT

Submitted, Biophysical Journal, ***Date***

Word count: ***Words***

Keywords:

Angiogenesis, extracellular matrix, computational modeling, matrix density, microvasculature, morphometry

Corresponding Author:

Jeffrey A. Weiss, Ph.D.

Department of Bioengineering
University of Utah
72 South Central Campus Drive, Rm. 2646

Salt Lake City, UT 84112

jeff.weiss@utah.edu

ABSTRACT

Angiogenesis, the process by which new blood vessels sprout off of existing vasculature, is heavily regulated by the mechanical interaction between endothelial cells within the sprout tip and the extracellular matrix (ECM). However, the mechanism as to how properties of the ECM regulate neovessel growth during sprouting angiogenesis is poorly understood. Computational models can be used to investigate this mechanism by allowing users to test hypothesis in ways not possible in the laboratory. The goal of this work was to characterize how matrix density regulates microvascular topology in an *in vitro* organ culture model of sprouting angiogenesis and then use these results to calibrate and validate a computational model. Using a three-dimensional (3D) culture of microvessel fragments within a collagen gel, it was observed that increasing matrix density resulted in poor angiogenic outgrowth and network formation. The computational model was capable at predicting these results by scaling neovessel growth and branching rate according to local matrix density. The accuracy of the computational model suggests that matrix density regulates the topology of the vascular network during angiogenesis by controlling the migration speed of endothelial cells and the frequency at which new sprouts arise due to branching. In addition to these observations, this work demonstrates the utility of computational models for investigating how changes in global experimental conditions affect microscopic interactions and consequently the final macroscopic topology of morphogenic processes such as angiogenesis.

INTRODUCTION

Vascular systems are essential in multicellular organisms for the distribution of oxygen and nutrients and removal of wastes. Without a functional vasculature, tissues engineered in the lab have been limited to the scale of effective diffusive transport (1). This limitation necessitates the ability to improve vascularization and direct vessels towards a desired vascular solution within tissue engineered devices. New vascular elements can be generated when new blood vessels sprout off of existing vasculature through a process known as angiogenesis. During angiogenesis, sprouting endothelial cells degrade the basement membrane by production of matrix metalloproteinases (MMPs) (2, 3) and migrate along components of the extracellular matrix (ECM) (4), resulting in neovessel elongation.

Recent studies have demonstrated that the biophysical interaction between neovessel sprouts and the ECM regulate the topology of vascular networks formed through angiogenesis (5-8). Cellular traction forces applied to the ECM create a stress field that cells detect and respond to (9, 10). The nature of the stress field is determined by the material properties of the matrix, such as fiber orientation and density, as well as geometry and boundary conditions. The relationship between angiogenesis and the mechanical properties of the ECM has been partially characterized using a three-dimensional (3D) organ culture model of microvessel fragments within a type-I collagen gel. In this model of sprouting angiogenesis, fragments cultured in a gel that was free to contract in all directions grew into a randomly oriented network (11, 12). When a mechanical boundary condition was imposed to prevent contraction of the gel, microvessels and collagen fibers were found aligned along the constrained axis (12).

Other studies have shown that the formation of capillary structures in cell culture models of angiogenesis is regulated by the density of the ECM. While studying human umbilical vein endothelial cells (HUVECs) undergoing capillary morphogenesis in a fibrin gel, Ghajar et al. observed reduced capillary length when the density of the fibrin matrix was increased (13, 14). Sieminski et al. showed that increasing the density of the type-I collagen matrix reduced growth and branching during capillary morphogenesis (15). Yamamura et al. observed reduced network formation with increased matrix density when studying bovine pulmonary microvascular endothelial cells (BPMECs) cultured on a collagen substrate (16). While these observations have been made using endothelial cells, changes in matrix density have not been investigated within an organ culture of microvessels which provides a more accurate representation of the true physiology.

The mechanism as to how matrix density regulates the topology of the vascular network is poorly understood. Experimental methods such as cell and organ cultures are useful, but in general only provide averaged information about the whole biological system limited to a single time point. While working within currently available experimental techniques, it is exceedingly difficult to establish a relationship between local cellular behavior and global characteristics of the biological system. Therefore, many researchers have turned to computational models to supplement experimental techniques, particularly within the field of angiogenesis research (17). Recently, a computational model of angiogenesis that uses ECM fiber orientation to determine the direction of microvessel growth has been proposed (18). This model prescribes the behavior of each individual neovessel sprout based on local ECM properties and has been shown to produce valid predictions of global morphometric data when compared to *in vitro* vascular networks. This computational model allows users to implement a hypothetical mechanism for

neovessel sprouts and compare the emergent prediction of vascular topology against analogous experimental data, providing researchers with the means to test hypotheses in ways that are not possible in the lab.

The objective of this study was to characterize how matrix density affects network topology within a 3D organ culture model of angiogenesis. The authors hypothesize that increasing matrix density will result in reduced angiogenesis as indicated by a reduction in network length and branching. The authors further hypothesize that the relationship between matrix density and global vascular topology can be accurately predicted using a computational model that adjusts the behavior of each individual neovessel according to local ECM density.

MATERIALS AND METHODS

In vitro model of angiogenesis

Vascularized constructs served as a model of *in vitro* angiogenesis and were prepared using methods described previously (19). Angiogenesis within these vascularized constructs has been extensively characterized in prior studies (11, 12). Constructs were prepared by seeding microvessel fragments within a 3D collagen gel. These fragments retain associated stroma cells and basement membrane after isolation and seeding. Sprouting of neovessel tips occurred in a spontaneous yet predictable fashion, with the first evidence of sprout tips usually observed by the second day of culture. The cultures were given media supplemented with vascular endothelial growth factor (VEGF) to assure a uniform presence of growth factors throughout the gel.

All reagents were obtained from Invitrogen (Carlsbad, CA) unless otherwise indicated. Epididymal fat pads were harvested from male retired breeder Sprague-Dawley rats in accordance to the University of Utah Institutional Animal Care and Use Committee. Fat pads were minced and subjected to partial digestion with 2.0 mg/mL Clostridium collagenase (Worthington Biochemicals, Lakewood, NJ). After four minutes, digestion was halted by the addition of Leibowitz (L-15) media and the solution was centrifuged. The pellet was washed, resuspended in media, and filtered through 350 μm and 30 μm sterile nylon filters sequentially. The filtration step removes undigested debris, single cells, and small fragments resulting in a population of microvessel fragments within a controllable range of sizes. At 35,000 per mL, vessel fragments were suspended within liquid type-I collagen solution (BD Biosciences, Bedford, MA) prepared at concentrations of 2.0, 3.0, or 4.0 mg/mL. For each of the three collagen solutions, 0.5 mL was transferred to a circular culture well (Nunc – Thermo Fisher Scientific, Rochester, NY, diameter = 15 mm) and allowed to polymerize into a three-dimensional gel (n = 4 gels per collagen concentration investigated, N = 12 gels total).

Serum-free growth media (20) was supplemented with 10.0 ng/mL rhVEGF (PeproTech, Rocky Hill, NJ) and provided to the cultures at day zero. Media and waste was removed every two days and replaced with 0.8 mL of fresh media. After six days of culture, the gels were fixed with 1.0 mL of 4% paraformaldehyde for 24 hours. Gels were then placed in a solution of 1x phosphate-buffered saline (DCF-PBS, pH 7.4) and 2.0 μg/mL Isolectin IB4-Alexa 488 to fluorescently label endothelial cells in preparation for confocal microscopy.

Confocal microscopy and skeletonization of vascular networks

Image data was collected from each vascularized construct by confocal microscopy using methods previously described (11, 12). Six adjacent fields at the geometric center of each gel were captured with an Olympus FV1000 microscope using a 10x objective and 488 nm laser. Each field was captured at a resolution of 512 x 512 pixels and was acquired to a depth of 200 μm at 2.5 μm intervals. The six fields were stitched together into a 2 x 3 grid using a custom software application, resulting in a mosaic image corresponding to a 3.8 x 2.5 x 0.2 mm region of the vascularized gel (Fig. 1 *A*). Processing and skeletonization of confocal data was performed using the image software Amira™ (Mercury Computer Systems, Carlsbad, CA). Mosaic stacks were subjected to a deconvolution routine (numerical aperture = 0.4, wavelength = 520 nm, refractive index of collagen = 1.35 (21)). A threshold value was calculated by fitting a Gaussian distribution to the image histogram, and this value was used in the automated skeletonization routine within Amira to decompose images of vessels down to a collection of line segments (Fig. 1 *B*). A custom software application was used to analyze the skeletonized vessel data and collect desired morphometric data (22). The particular morphometrics collected from vascularized constructs were the *total vascular length*, the degree of *network interconnectivity*, the number of *branching points*, and the number of *end points*.

The collective length of all microvessels within the imaged domain was defined as the *total vascular length*. This morphometric can also be described as the contour length of the network, and it is useful as a metric of overall angiogenic outgrowth during the culture period. Neovessels sprouting from fragments were observed to form continuous vascular networks, with inter-vessel connections presumably formed through anastomosis. The extent of vascular perfusion was determined by calculating the *network interconnectivity*, or the percentage of microvessels that fused into a single continuous vascular network. The network interconnectivity for a particular

culture was calculated by measuring the length of the longest continuous microvessel tree and normalizing by the total vascular length. A *branching point* was defined as a node connected to 3 different line segments and indicates either a new vessel sprout (branching) or two separate vessels fusing into one (anastomosis). *End points* are terminal ends of vessels, defined by a node that is associated with only one segment. Measuring the number of end points quantifies the amount of active growth tips and characterizes the degree of branching and anastomosis occurring within the domain.

Computational growth model

A computational model of microvessel growth capable of predicting 3D vessel morphology during spontaneous angiogenesis was utilized to simulate the *in vitro* experiments (Fig. 1 *C*). This growth model has been shown to make valid predictions of angiogenesis within isotropic or anisotropic matrix (18, 23, 24) using information about the ECM to determine neovessel length, direction, and branching. A simulation domain corresponding to the imaged region of each vascularized gel (3.8 x 2.5 x 0.2 mm) was fit with a regular quadrilateral grid. Properties of the ECM field that influence angiogenic vessel growth, such as fiber orientation and matrix density, were stored at the nodes of the grid. A collagen fiber orientation value between 0 and π radians was randomly generated at each node in the grid. Initial microvessel fragments were represented as line segments and seeded throughout the domain with random positions and orientations.

At each time step, vessel growth was simulated by creating new line segments at the positions of all active growth tips. The direction of each new line segment, ψ_{new}, was determined by a weighted average of the parent vessel's direction, ψ_{parent}, and the directional component determined by collagen fiber guidance, θ:

$$\psi_{new} = w_1\psi_{parent} + w_2\theta \quad \textbf{(Eq. 1)}$$
$$w_1 = 0.91$$
$$w_2 = 0.09$$

The values for the weights w_1 and w_2 were selected in order to create microvessels with a similar morphology to those seen *in vitro*. The component of neovessel direction determined by collagen fiber guidance, $\boldsymbol{\theta}$, was interpolated using trilinear shape functions through the following equation:

$$\theta(\boldsymbol{x}) = \sum_{j=1}^{8} \theta_j N_j(\boldsymbol{x}) \quad \textbf{(Eq. 2)}$$

In Eq. 2, $\boldsymbol{\theta}_j$ is the collagen fiber orientation value stored at node j of the grid element in which the growth tip resides. N_j is the value of the shape function for node j at the position of the active growth tip, $\boldsymbol{x}$.

Branching, the sprouting of a neovessel off of an existing vessel, was modeled as a random process. During a time step, each segment generated a number between 0 and 1. If the random number exceeded the branching probability (b_0 = 0.1), that segment would form a branch. Anastomosis, the fusing of two vessels into one, was permitted for all active growth tips. If a growth tip was within 25 μm of another vessel, the vessels anastomose by creating a new line segment connecting the two points. After which, all growth tips involved during the anastomosis were then inactivated.

In order to implement vessel growth that was sensitive to matrix density, a scaling factor was calculated from experimental data by taking the average total vascular length for each culture

condition (2.0, 3.0, and 4.0 mg/mL) and normalizing by the average total vascular length measured in the 3.0 mg/mL constructs. Values of the scaling factor *v* were then fit to a three-parameter exponential function that described how the factor changed with collagen density:

$$v = v_0 + a_0 e^{-a_1 c} \quad \textbf{(Eq. 3)}$$
$$2.0 \le c \le 4.0$$
$$a_1 > 0$$

In Eq. 3 above, *v* was the scaling factor, *c* was the collagen concentration (mg/mL), and v_0, a_0, and a_1 were parameters determined by the curve fit. The computational model accepted the collagen concentration of the matrix as an input parameter and calculated the corresponding scaling factor using Eq. 3. The scaling factor was used to proportionally scale two growth mechanisms. As the density of the matrix increased, the scaling factor reduced the length of new line segments and probability of each segment forming a branch.

Simulations of the *in vitro* experiments were performed in order validate the computational framework (n = 4 simulations per culture condition, N = 12 simulations total). The number of initial fragments in the simulations (N_{frag} = 70) was determined from the volume of the domain and the seeding density (35,000 frags/mL). For each culture condition, morphometric data from the computational simulations (total vessel length, network interconnectivity, number of branch points, and number of end points) were compared to values measured from the corresponding experimental cultures.

Assessment of statistical significance

For a given morphometric, single-factor ANOVA testing (α = 0.05) was performed on either experimental or simulation data across collagen concentration to determine significance. A two-tailed student's T-test for populations with unequal variance (α = 0.05) was used to assess statistical significance between experimental data and computational predictions for a given matrix density level.

RESULTS

Experimental Results

Angiogenic sprouting and neovessel outgrowth occurred was consistent within all microvessel cultures. Well-established microvasculature was observed at day six for all matrix density conditions. The circular, free-floating vascularized gels experienced significant contraction during the six-day culture period, with construct diameters reduced by an average of 40.0 ± 5.0%, 20.0 ± 5.0%, and 7.0 ± 1.0% for 2.0, 3.0, and 4.0 mg/mL gels, respectively (average ± std dev). Qualitatively, the highest levels of angiogenesis occurred in the 2.0 mg/mL constructs, while angiogenesis within the 4.0 mg/mL constructs was significantly reduced (Fig. 2 *A*-*C*).

Measurements of total vascular length within the vascularized constructs indicate a reduction in overall neovessel outgrowth as the density of the matrix was increased (Fig. 3 *A black*) (ANOVA, $P < 0.05$). A decrease in network interconnectivity indicates that increasing the density of the matrix results in more discontinuous vascular networks (Fig. 3 *B black*) (ANOVA, $P < 0.05$).

Other angiogenic neovessel behaviors, such as branching and anastomosis, were characterized by measuring the number of branch points and end points within the vascularized constructs. After six days in culture, the number of branch points was observed to decrease as the density of the collagen matrix increased (Fig. 4 *A black*) (ANOVA, $P < 0.05$). Similarly, the number of end points decreased with increased matrix density (Fig. 5 *A black*) (ANOVA, $P < 0.05$). However, these measurements do not account for the reduction of construct volume due to contraction observed to occur over the six day culture period.

Increased contraction of low-density gels could lead to the increased amount of branch points and end points due to more microvessels being pulled into the field of view. Therefore branch point and end point data were normalized by total vascular length to isolate the tendency of microvessels to form a branch or free end per unit length of growth. As the density of the matrix increased, microvessels were observed to form less branch points per unit length of growth (Fig. 4 *B black*) (ANOVA, $P < 0.05$). The amount of free ends per unit length was observed to increase as matrix density increased (Fig. 5 *B black*) (ANOVA, $P < 0.05$).

Computational Results

The computational growth model was successful at predicting angiogenesis for all matrix density conditions. The scaling factor v was used to scale growth rate and branching probability according to the density of the matrix. In order to calculate this scaling factor, the average total vascular length measured from 2.0, 3.0, and 4.0 mg/mL gels was normalized by the average total vascular length for 3.0 mg/mL constructs (making $v = 1.0$ for a concentration of 3.0 mg/mL). A three-parameter exponential function was fit to the normalized length data (Eq. 3, $R^2 = 1.0$), providing a function that returned a scaling factor value given a particular collagen concentration

(Fig. 6). The parameters determined by this curve fit were v_0 = 0.2417, a_0 = 4.8573, and a_1 = 0.6190. The inclusion of density scaling into these mechanisms resulted in distinct qualitative differences among predictions of angiogenesis across the different matrix density conditions (Fig. 2 *D*-*F*).

The computational framework was capable of predicting accurate morphometric data across changes in matrix density. Simulations accurately predicted a reduction in total vascular length as the density of the matrix increased (Fig. 3 *A grey*) (ANOVA, $P < 0.05$). Microvasculature predicted by the growth model became increasing discontinuous as matrix density increased in a trend similar to that seen *in vitro* (Fig. 3 *B grey*) (ANOVA, $P < 0.05$).

Less branching points were measured from the computational simulations as the density of the matrix increased (Fig. 4 *A grey*) (ANOVA, $P < 0.05$), and branching per unit length followed a similar trend (Fig. 4 *B grey*) (ANOVA, $P < 0.05$). Free ends measured from computational predictions decreased with increased matrix density (Fig. 5 *A grey*) (ANOVA, $P < 0.05$), and measurements of end points per unit length increased along with matrix density (Fig. 5 *B grey*). Unless otherwise indicated, morphometric data from computational predictions were statistically indistinguishable from experimental measurements through T-test. The only exception occurred when comparing normalized end points from 2.0 mg/mL collagen gels, for which the experimental data and simulation predictions were statistically distinguishable ($P < 0.05$, indicated by star and bracket in Fig. 5 *B*).

DISCUSSION

This work demonstrated a computational framework that was capable of accurately predicting microvascular network topology as a function of initial ECM density. As the density of the matrix was increased, the computational model predicted neovasculatures with shorter contour lengths, reduced branching per unit length, more free ends per unit length, and reduced connectivity (Fig. 3, 4, 5). These predictions were compared against measurements from experimental cultures of angiogenic microvessels to demonstrate validity. For all but one of the cases, morphometric data from the computational model at a given level of matrix density were statistically indistinguishable from comparable experimental measurements by T-test.

Increasing matrix density within the microvessel cultures caused a reduction in neovascularization (Fig. 2), confirming the initial hypothesis. During angiogenesis, traction forces applied by neovessel sprouts create a stress field within the matrix. The state of stress is determined by the material properties and geometry of the matrix. Changing the density of the matrix drastically changes the state of stress that neovessels experience during angiogenesis, leading to significantly altered topology of the final vascular network. Networks cultured in high density matrix had a shorter contour length after the six day culture period (Fig. 3 *A black*), suggesting that increased matrix density significantly decreases neovessel growth rate. Networks cultured in high density matrix were less divergent than their lower-density counterparts, seen in a reduction in the number of branch points formed per unit length of growth (Fig. 4 *black*). An increase in matrix density also resulted in an increase in the number of free ends per unit length (Fig. 5 *black*). As the density of the matrix increased, the observation of increased free ends despite a decreased amount of branching suggests anastomosis occurred less frequently. A slower growth rate reduces the chance of neovessels finding a potential anastomosis partner resulting in poor network formation (Fig. 3 *B black*).

The computational model was capable of predicting similar trends in neovascular topology by adjusting neovessel growth rate and the probability of branch formation according to local matrix density. A scaling factor was calculated from experimental data and used to adjust growth rate and branching probability. An exponential function was chosen to calculate the scaling factor as it was observed that length and branching morphometric data exhibited an exponential trend with matrix density (Eq. 3). The averaged total vascular length at each density level surveyed during the experiments was normalized by the total vascular length of the 3.0 mg/mL constructs, providing the factor by which total vascular length changes across a change in matrix density (Fig. 6). The scaling factor had a value less than 1.0 for matrix densities greater than 3.0 mg/mL and a value greater than 1.0 for matrix densities less than 3.0 mg/mL. During each growth step, the model surveyed the density of the ECM and calculated the scaling factor which adjusted the length of each new segment and the probability of each segment forming a new branch accordingly.

The accuracy of the computational model suggests that matrix density regulates the topology of the vascular network during angiogenesis by controlling the rate of growth and branch formation. Increasing the concentration of collagen protein has been shown to result in gels with increased fiber density and greater mechanical stiffness (25-29). In this study, it was observed that increasing collagen density in vascularized constructs while keeping vessel density constant led to less compaction over the 6 day culture period. These results suggest that the magnitude of traction forces applied by endothelial cells remains unchanged as matrix density increases. Using HUVECs in a fibrin gel, Ghajar et al. observed that increasing the density of the matrix resulted in no noticeable increase in MMP-2 and -9 activities (13), two important soluble proteins responsible for matrix proteolysis during angiogenesis (30-33). With no accompanying

increase in traction force magnitude or proteolytic activity, increasing the density renders the matrix more difficult for endothelial cells to deform and remodel, impeding migration and reducing the rate of angiogenic outgrowth. This observation is supported by the work of both Sieminski et al. and Yamamura et al. in which it was observed that capillary morphogenesis was regulated by the apparent stiffness of the matrix (15, 16).

Increasing the density of the matrix was also observed to reduce the rate of branch formation during angiogenesis. Ghajar et al. made similar observations of reduced sprouting upon increasing the density of the matrix (13, 14). These observations were made using HUVECs cultured on microspheres within a fibrin matrix. A feeder layer of fibroblasts was cultured on top of the matrix to serve as a source of growth factors. Ghajar et al. proposed that increasing matrix density reduced sprouting by decreasing the porosity of matrix and hindering the diffusion of soluble growth factors (13). This conclusion was supported by the observation that co-culturing fibroblasts within the matrix along with endothelial cells improved sprouting (13). In the co-culture model, the fibroblasts acted as pseudo-stroma cells and the length over which growth factors had to diffuse over to reach the endothelial cells was drastically reduced. However, the experimental observations presented in this work do not support the conclusion proposed by Ghajar et al. In these experiments, an organ culture model of microvessels within collagen gel exhibited a similar trend of reduced angiogenesis across increases in matrix density. Endothelial cells within this culture model remain intact as microvessel fragments and retain their association with stroma cells (perictyes) and the basement membrane. Therefore, the diffusive length between neovessel sprouts and the stroma was small. Additionally, the growth media for these cultures was supplemented with VEGF in order to ensure a uniform presence of growth factor throughout the gel. The inverse relationship between neovessel sprouting and

matrix density observed with this organ culture model suggests the existence of an additional mechanism, independent from chemotaxis, by which matrix density regulates angiogenic sprouting.

Recent research suggests the additional mechanism regulating neovessel sprouting is mechanical in nature (34). Korff and Augustin observed that tensional forces within the ECM control sprouting (35). The fibrillar structure of the ECM serves as the major pathway for mechanotransduction between neovessels, and therefore the properties of the ECM regulate the state of stress experienced by the cellular population. As the density of the matrix increases, the stiffness of the ECM increases but the magnitude of traction forces applied by endothelial cells remains unchanged. Therefore, the magnitude of the stress field within the ECM was reduced upon an increase of matrix density. Reducing the ECM stress field reduces the magnitude of tensional forces experienced by the neovessels during angiogenesis, which leads to reduced sprouting. Other authors have suggested that the ECM stress field plays a role during angiogenic sprouting as well. Ingber proposed that stress concentrations within the ECM cause vessels to form a new sprout (36). Additionally, a computational model of angiogenesis proposed by Bauer et al. suggested that steep gradients in matrix density can lead to stress concentrations which cause sprouting (37). However, there is still much about the mechanical interaction between neovessels and the ECM during angiogenesis that is not well understood. For example, there has been no mechanistic description as to how global changes in matrix boundary conditions or applied loads affect the sprouting, orientation, and growth of new microvessels.

Computational models provide a means for investigating the role of this mechanical interaction during angiogenesis. The model outlined in this work was able to elucidate how ECM density

regulates neovessel behavior during angiogenesis. However, the model has limitations. During the simulations, the matrix density and fiber orientation fields were considered to be constant throughout time, which does not accurately represent how the matrix changes during angiogenesis. Kirkpatrick et al. observed collagen remodeling during angiogenesis and found that sprout tips condense the matrix and alter fiber orientation via traction forces (38). Therefore, the computational model outlined in this study can be further improved by including a framework in solid mechanics to update properties of the ECM throughout time in response to deformation caused by cellular traction forces. For example, the conservation of mass describes how matrix density will change during contraction of gel volume. The deformation gradient tensor, the primary measure of deformation in the theories of kinematics, provides a linear transformation rule describing how free vectors representing the orientation of ECM fibers transform during matrix remodeling (39). Coupling the growth model with the field theories of continuum mechanics will provide a simulation framework for studying how mechanical forces and ECM structure at the microscale influence growth and proliferation of vessels at the macroscale. Such a framework would allow investigators to establish cause-and-effect relationships between global changes at the tissue level and local cellular response, and vice versa.

In summary, it was observed that increasing the density of the ECM significantly reduced angiogenesis and network formation. The computational framework outlined in this study was capable of predicting this trend by adjusting neovessel growth rate and branching probability according to local ECM density. In future work, this computational framework can be improved by including a framework in solid mechanics in order to couple vessel growth with matrix deformation. This coupled computational framework will allow investigators to study how

changing the matrix at the macroscale can be used to direct angiogenesis towards producing desired vascular solutions.

REFERENCES

1. Obradovic, B., R. L. Carrier, G. Vunjak-Novakovic, and L. E. Freed. 1999. Gas exchange is essential for bioreactor cultivation of tissue engineered cartilage. Biotech. Bioeng. 63:197-205.
2. Fisher, C., S. Gilbertson-Beadling, E. A. Powers, G. Petzold, R. Poorman, and M. A. Mitchell. 1994. Interstitial collagenase is required for angiogenesis in vitro. Dev. Biol. 162:499-510.
3. Haas, T. L., S. J. Davis, and J. A. Madri. 1998. Three-dimensional type I collagen lattices induce coordinate expression of matrix metalloproteinases MT1-MMP and MMP-2 in microvascular endothelial cells. J. Biol. Chem. 273:3604-3610.
4. Vernon, R. B., and E. H. Sage. 1999. A novel, quantitative model for study of endothelial cell migration and sprout formation within three-dimensional collagen matrices. . Microvasc. Res. 57:118-133.
5. Rivilis, I., M. Milkiewicz, P. Boyd, J. Goldstein, M. D. Brown, S. Egginton, F. M. Hansen, O. Hudlicka, and T. L. Haas. 2002. Differential involvement of MMP-2 and VEGF during muscle stretch- versus shear stress-induced angiogenesis. . Am. J. Physiol. Heart Circ. Physiol. 283:H1430-H1438.
6. Tranqui, L., and P. Tracqui. 2000. Mechanical signalling and angiogenesis. The integration of cell- extracellular matrix couplings. C.R. Acad. Sci. Paris Life Sci. 323:31-47.
7. Vailhe, B., X. Ronot, P. Tracqui, Y. Usson, and L. Tranqui. 1997. In vitro angiogenesis is modulated by the mechanical properties of fibrin gels and is related to alpha(v)beta3 integrin localization. In Vitro Cell Dev. Biol. Anim. 33:763-773.
8. Vernon, R. B., and E. H. Sage. 1996. Contraction of fibrillar type I collagen by endothelial cells: a study in vitro. J. Cell. Biochem. 60:185-197.
9. Hur, S. S., Y. Zhao, Y. S. Li, E. Botvinick, and S. Chen. 2009. Live cells exert 3-dimensional traction forces on their substrata. Cell. Mole. Bioeng. 2:425-436.
10. Lopez, J. I., J. K. Mouw, and V. M. Weaver. 2008. Biomechanical regulation of cell orientation and fate. Ocogene 27:6981-6993.
11. Krishnan, L., J. B. Hoying, H. Nguyen, H. Song, and J. A. Weiss. 2007. Interaction of angiogenic microvessels with the extracellular matrix. Am. J. Physiol. Heart Circ. Physiol. 293:H3650-3658.
12. Krishnan, L., C. J. Underwood, S. Maas, B. J. Ellis, T. C. Kode, J. B. Hoying, and J. A. Weiss. 2008. Effect of mechanical boundary conditions on orientation of angiogenic microvessels. Cardiovasc. Res. 78:324-332.
13. Ghajar, C. M., X. Chen, J. W. Harris, V. Suresh, C. C. Hughes, N. L. Jeon, A. J. Putnam, and S. C. George. 2008. The effect of matrix density on the regulation of 3-D capillary morphogenesis. Biophys. J. 94:1930-1941.
14. Ghajar, C. M., S. C. George, and A. J. Putnam. 2008. Matrix Metalloproteinase Control of Capillary Morphogenesis. Crit. Rev. Eukaryot. Gene Expr. 18:251-278.
15. Sieminski, A. L., R. P. Hebbel, and K. J. Gooch. 2004. The relative magnitudes of endothelial force generation and matrix stiffness modulate capillary morphogenesis in vitro. Exp. Cell Res. 297:574-584.

16. Yamamura, N., R. Sudo, M. Ikeda, and K. Tanishita. 2007. Effects of the Mechanical Properties of Collagen Gel on the In Vitro Formation of Microvessel Networks by Endothelial Cells. Tissue Eng. 13:1443-1453.
17. Peirce, S. M. 2008. Computational and mathematical modeling of angiogenesis. Microcirculation 15:739-751.
18. Edgar, L. T., S. Sibole, C. J. Underwood, J. Guilkey, and J. A. Weiss. 2011. A Computational Model of In Vitro Angiogenesis based on Extracellular Matrix Fiber Orientation. Comp. Meth. Biomech. Biomed. Eng. In Revision.
19. Hoying, J. B., C. A. Boswell, and S. K. Williams. 1996. Angiogenic potential of microvessel fragments established in three-dimensional collagen gels. In Vitro Cell Dev. Biol. Anim. 32:409-419.
20. Bottenstein, J. E., and G. H. Sato. 1979. Growth of a rat neuroblastoma cell line in serum-free supplemented medium. Proc. Natl. Acad. Sci. USA 76:514-517.
21. Liu, Y., M. Griffith, M. A. Watsky, J. V. Forrester, L. Kuffova, D. Grant, K. Merrett, and D. J. Carlsson. 2006. Properties of porcine and recombinant human collagen matrices for optically clear tissue engineering applications. Biomacromolecules 7:1819-1828.
22. WinFiber3D, http://mrl.sci.utah.edu.
23. Sibole, S., C. J. Underwood, J. Guilkey, and J. A. Weiss. 2008. A discrete computational model to predict in vitro angiogenesis. In ASME Sum. Bioeng. Conf. 2008.
24. Sibole, S., C. J. Underwood, J. Guilkey, and J. A. Weiss. 2009. A continuous-discrete mathematical model simulates in vitro angiogenesis. In ASME Sum. Bioeng. Conf. 2009.
25. Nicosia, R. F., and A. Ottinetti. 1990. Modulation of microvascular growth and morphogenesis by reconstituted basement membrane gel in three-dimensional cultures of rat aorta: a comparative study of angiogenesis in matrigel, collagen, fibrin, and plasma clot. In Vitro Cell Dev. Biol. 26:119-128.
26. Nicosia, R. F., and A. Ottinetti. 1990. Growth of microvessels in serum-free matrix culture of rat aorta. A quantitative assay of angiogenesis in vitro. Lab Invest. 63:115-122.
27. Krishnan, L., J. A. Weiss, M. D. Wessman, and J. B. Hoying. 2004. Design and application of a test system for viscoelastic characterization of collagen gels. Tissue Eng. 10:241-252.
28. Roeder, B. A., K. Kokini, J. E. Sturgis, J. P. Robinson, and S. L. Voytik-Harbin. 2002. Tensile mechanical properties of three-dimensional type I collagen extracellular matrices with varied microstructure. J. Biomech. Eng. 124:214-222.
29. Wood, G. C., and M. K. Keech. 1960. The formation of fibrils from collagen solutions. 1. The effect of experimental conditions: kinetic and electron-microscope studies. Biochem. J. 75:588-598.
30. Sternlicht, M. D., and Z. Werb. 2001. How matrix metalloproteinases regulate cell behavior. Annu. Rev. Cell Dev. Biol. 17:463-516.
31. Page-McCaw, A., A. J. Ewald, and Z. Werb. 2007. Matrix metalloproteinases and the regulation of tissue remodelling. Nat. Rev. Mol.Cell Biol. 8:221-233.
32. Visse, R., and H. Nagase. 2003. Matrix metalloproteinases and tissue inhibitors of metalloproteinases: structure, function, and biochemistry. Circ. Res. 92:827-839.
33. Bergers, G., R. Brekken, G. McMahon, T. H. Vu, T. Itoh, K. Tamaki, K. Tanzawa, P. Thorpe, S. Itohara, Z. Werb, and D. Hanahan. 2000. Matrix metalloproteinase-9 triggers the angiogenic switch during carcinogenesis. Nat. Cell Biol. 2:737-744.

34. Shiu, Y. T., J. A. Weiss, J. B. Hoying, M. N. Iwamoto, I. S. Joung, and C. T. Quam. 2005. The role of mechanical stresses in angiogenesis. Crit. Rev. Biomed. Eng. 33:431-510.
35. Korff, T., and H. Augustin. 1999. Tensional forces in fibrillar extracellular matrices control directional capillary sprouting. J. Cell Sci. 112:3249-3258.
36. Ingber, D. 2002. Mechanical Signaling and the Cellular Response to Extracellular Matrix in Angiogenesis and Cardiovascular Physiology. Circ. Res. 91:877-887.
37. Bauer, A., T. L. Jackson, and Y. Jiang. 2009. Topography of Extracellular Matrix Mediates Vascular Morphogenesis and Migration Speeds in Angiogenesis. PLOS Comp. Biol. 5.
38. Kirkpatrick, N. D., S. Andreou, J. B. Hoying, and U. Utzinger. 2007. Live imaging of collagen remodeling during angiogenesis. Am. J. Physiol. Heart Circ. Physiol. 292:H3198-3206.
39. Holzapfel, G. 2000. Nonlinear Solid Mechanics: A Continuum Approach for Engineering. John Wiley & Sons, LTD.

FIGURE LEGENDS

Figure 1. Visualization of *in vitro* experiments and simulation results. (A) Z-projection image of microvessels cultured in a 3.0 mg/mL collagen gel after day 6 of culture. Endothelial cells within the culture were labeled with Isolectin IB4-Alexa 488 and imaged using a confocal microscope with a 10x objective. (B) Skeletonized vessel data obtained from confocal image data of a vascularized collagen gel. All image processing was performed using Amira™ (Mercury Computer Systems, Carlsbad, CA). (C) Results of a simulation using the computational model. Microvessels were represented as a collection of line segments, and growth was simulated by the addition of new segments to the free ends of existing segments. (Scale bar = 350 μm).

Figure 2. Microvasculatures observed at different levels of collagen density. Confocal images of vascularized collagen gels taken at day 6 of growth are presented on the top. Results of the comparable computational simulations are presented as volume-rendered line segment data along the bottom. The three levels of collagen density assessed in this study were: 2.0 mg/mL (A, D), 3.0 mg/mL (B, E), and 4.0 mg/mL (C, F). (Scale bar = 350 μm).

Figure 3. Increasing the density of the matrix reduced angiogenic outgrowth and network formation. (A) The total vascular length was calculated by taking the sum of the lengths of all microvessels within the domain. As matrix density increased, it was observed that total vascular length decreased. Measurements from the experimental cultures are presented in black and predictions from the computational model are presented in gray. (B) Vessel interconnectivity

was calculated by taking the length of the longest continuous microvessel tree and dividing this value by the total vascular length. Vessel interconnectivity indicates the percentage of microvessels within the domain that are connected into the largest continuous vascular network. Increasing the density of the matrix led to decreased vessel interconnectivity, indicating a reduction in network formation. For all cases, morphometric values predicted by the computational simulations were statistically indistinguishable from experimental measurements through T-test.

Figure 4. A branching point was defined as any node that connected to three or more vessel segments. Branching points were created by either a new vessel sprout (branching) or two separate vessels fusing into one (anastomosis). Measurements from the experimental cultures are presented in black and predictions from the computational model are presented in gray. (A) As matrix density increased, the number of branch points decreased. However, these observations could be skewed by the increased amount of contraction in the more compliant collagen gels. Increased contraction would result in more vessels being pulled into the field of view, which could result in the observed increase in the number of branching points. (B) The number of branch points was normalized by the total vascular length in order to isolate the tendency of microvessels to form a branch point per unit length of growth. Branching per unit length was observed to decrease as matrix density was increased. For all cases, morphometric values predicted by the computational simulations were statistically indistinguishable from experimental measurements through T-test.

Figure 5. An end point was defined as a node that was associated with only one vessel segment and represents an active growth tip. Measurements from the experimental cultures are presented in black and predictions from the computational model are presented in gray. (A) The amount of end points was observed to decrease as matrix density increased. (B) However, normalizing the number of end points by the total vascular length revealed that the number of free ends per unit length increased along with matrix density. For all but one of the cases, morphometric values predicted by the computational simulations were statistically indistinguishable from experimental measurements through T-test. The exception occurred with normalized end points for the 2.0 mg/mL collagen gels ($P < 0.05$, indicated by star and bracket).

Figure 6. A scaling factor was calculated from experimental data and used to scale growth rate and branching probability within the computational model based on local ECM density. The factor was calculated by taking the average total vascular length measured for the 2.0, 3.0, and 4.0 mg/mL vascularized constructs and normalizing by the total vascular length for the 3.0 mg/mL construct. Experimental data is presented as the solid points on the graph. This data was then fit to the exponential function described in Eq. 3 ($R^2 = 1.0$). The fitted function is presented as the dashed line on the graph.

Figure 1. (column width)

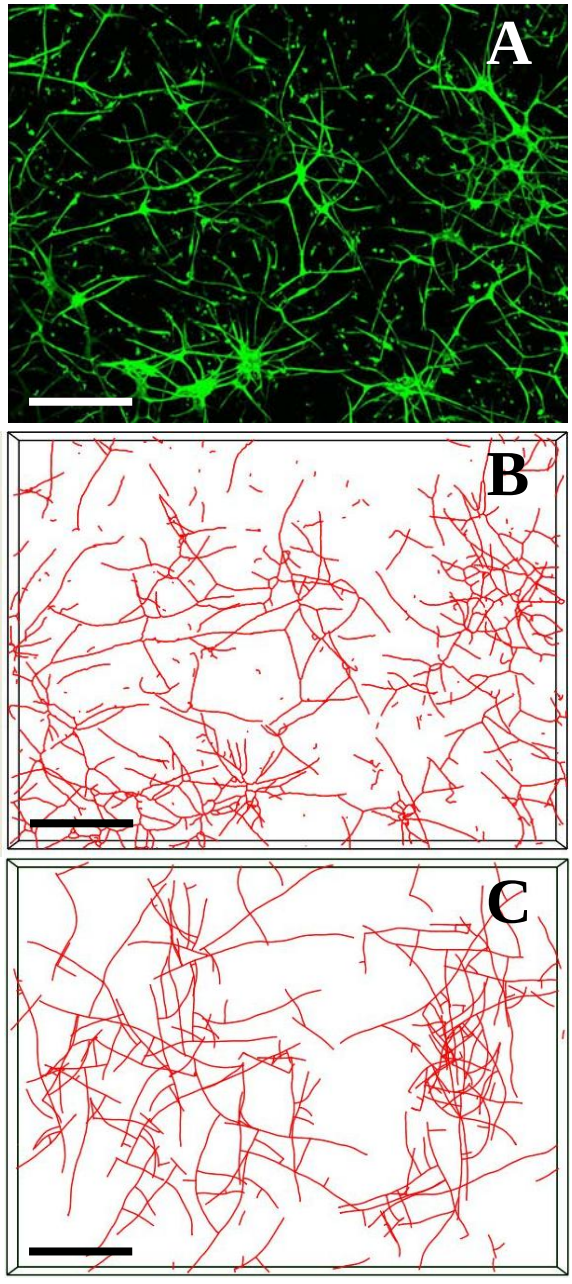

Figure 2. (page width)

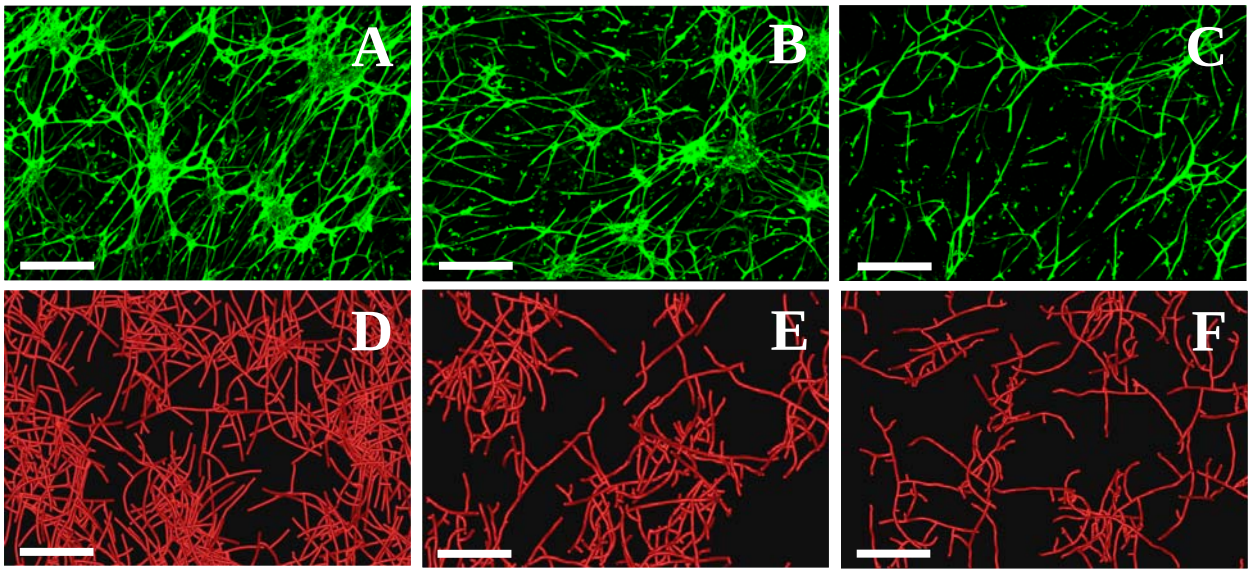

Figure 3. (column width)

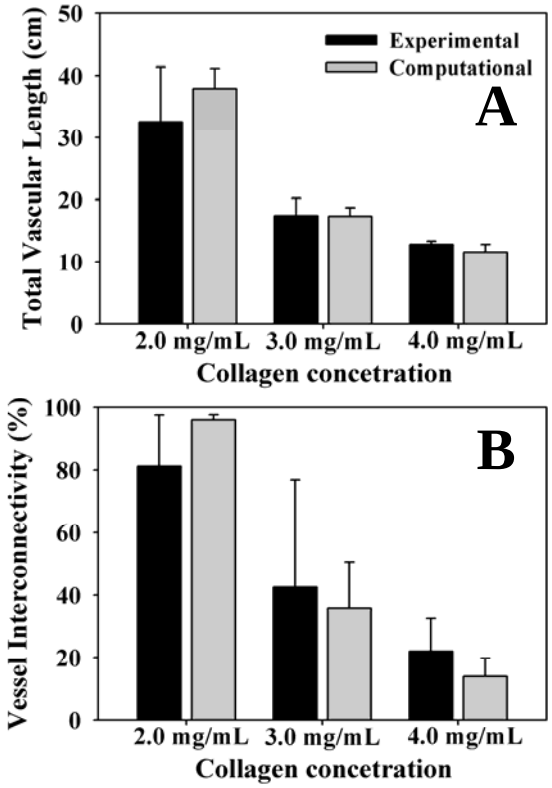

Figure 4. (column width)

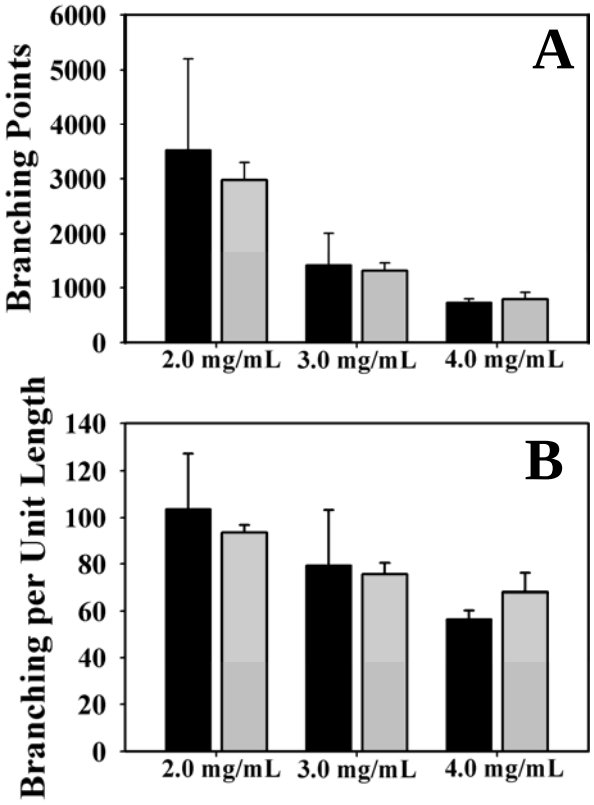

Figure 5. (column width)

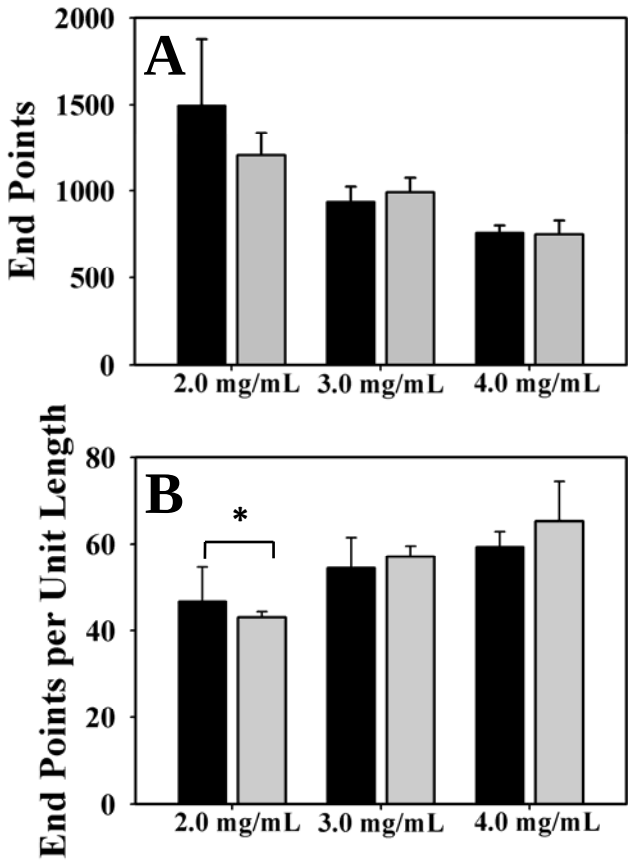

Figure 6. (column width)